Steady-State Kinetic Mechanism of *Escherichia coli* UDP-*N*-Acetylenolpyruvylglucosamine Reductase

Adil M. Dhalla,[‡] Joseph Yanchunas, Jr.,[‡] Hsu-Tso Ho,[§] Paul J. Falk,[§] Joseph J. Villafranca,[‡] and James G. Robertson*,[‡]

Enzymology Laboratory, Division of Macromolecular Structure, Bristol-Myers Squibb Pharmaceutical Research Institute, Princeton, New Jersey 08543-4000, and Department of Microbiology, Bristol-Myers Squibb Pharmaceutical Research Institute, Wallingford, Connecticut 06492-7660

Received December 1, 1994; Revised Manuscript Received February 13, 1995[⊗]

ABSTRACT: The *Escherichia coli* MurB gene encoding UDP-*N*-acetylenolpyruvylglucosamine reductase was expressed to a level of ≈100 mg/L as a fusion construct with maltose binding protein. Rapid affinity purification, proteolysis, and anion exchange chromatography yielded homogeneous enzyme containing 1 mol/mol bound FAD. Enzyme was maximally activated by K^+, NH_4^+, and Rb^+ at cation concentrations between 10 and 50 mM. Steady-state enzyme kinetics at pH 8.0 and 37 °C revealed weak and strong substrate inhibition by NADPH and UDP-*N*-acetylenolpyruvylglucosamine, respectively, where the K_is were 910 μM and 73 μM. Substrate inhibition was pH dependent for both substrates. Initial velocity measurements as a function of both substrates produced patterns consistent with a ping pong bi bi double competitive substrate inhibition mechanism. Data at pH 8.0 yielded kinetic constants corresponding to $K_{m,UNAGEP} = 24 \pm 3$ μM, $K_{i,UNAGEP} = 73 \pm 19$ μM, $K_{m,NADPH} = 17 \pm 3$ μM, $K_{i,NADPH} = 910 \pm 670$ μM, and $k_{cat} = 62 \pm 3$ s^{-1}. A slow anaerobic exchange reaction with thio-$NADP^+$ provided evidence for release of $NADP^+$ in the absence of UNAGEP. Alternate reduced nicotinamide dinucleotides, including NHXDPH, 3′-NADPH, and α-NADPH, were substrates, whereas NADH was not. Several nucleotides, including ADP and UDP, were weak inhibitors of the enzyme with inhibition constants between 5 and 97 mM. Various analogs of $NADP^+$, including 3′-$NADP^+$, thio-$NADP^+$, $APADP^+$, $NEthDP^+$, and $NHXDP^+$, were inhibitors of the enzyme with respect to NADPH and yielded inhibition constants in the range of 110−1100 μM. Analogs without the 2′- or 3′-phosphate of NADPH or $NADP^+$ were not substrates or inhibitors. Double inhibition experiments with varied $APADP^+$ and UNAG produced inhibition patterns consistent with mutually exclusive inhibitor binding. The data suggest that NADPH and UNAGEP share a subsite that prevents both molecules from binding at once.

Uridine diphospho-*N*-acetylenolpyruvylglucosamine reductase (EC 1.1.1.158) catalyzes the second step in the biosynthetic pathway responsible for assembly of the bacterial cell wall UDP-*N*-acetylmuramic acid pentapeptide (Bugg & Walsh, 1993). The reaction transfers two electrons from NADPH to the enolpyruvyl moiety of UNAGEP,[1] as illustrated in Figure 1, where enzyme bound FAD serves as the redox intermediate (Benson et al., 1993). After reduction of the enolpyruvyl moiety, the free carboxylate becomes the reactive center for the next enzyme in the pathway, which forms a peptide bond between UNAM and alanine. Successive enzymes ligate D-glutamate, *meso*-diaminopimelate, and D-Ala-D-Ala to the growing chain to complete the UNAM pentapeptide. The assembled pentapeptide undergoes further transpeptidation, lipid modification, polysaccharide conjugation, and, finally, transport out of the cell for incorporation into the peptidoglycan layer of the cell wall. Biosynthesis of the UNAM pentapeptide provides an essential precursor for bacterial proliferation, but despite the importance of this pathway, the reactions have not been studied extensively due to the limited available amounts of pure enzymes and substrates.

Recently, however, the MurA (Marquardt et al., 1992), MurB (Pucci et al., 1992), MurC (Ikeda et al., 1990a), and MurD (Mengin-Lecreulx & van Heijenoort, 1990; Ikeda et al., 1990b) genes encoding the first four enzymes in the pathway have been cloned and sequenced. This has made it possible to begin expressing significant amounts of these

* To whom correspondence should be addressed.
‡ Division of Macromolecular Structure, Bristol-Myers Squibb Pharmaceutical Research Institute, Princeton, NJ.
§ Department of Microbiology, Bristol-Myers Squibb Pharmaceutical Research Institute, Wallingford, CT.
⊗ Abstract published in *Advance ACS Abstracts,* April 1, 1995.

[1] Abbreviations: ADP, adenosine diphosphate; ADP-ribose, adenosine 5′-diphosphoribose; APADPH, 3-acetylpyridine adenine dinucleotide phosphate reduced form; $APADP^+$, 3-acetylpyridine adenine dinucleotide phosphate; α-NADPH, α-nicotinamide adenine dinucleotide phosphate reduced form; α-$NADP^+$, α-nicotinamide adenine dinucleotide phosphate; IPTG, isopropyl β-D-thiogalactopyranoside; MA, muramic acid; NAG, *N*-acetylglucosamine; NAGP, *N*-acetylglucosamine 1-phosphate; NAMA, *N*-acetylmuramic acid; NEthDPH, nicotinamide 1,N^6-ethenoadenine dinucleotide phosphate reduced form; $NEthDP^+$, nicotinamide 1,N^6-ethenoadenine dinucleotide phosphate; NHXDPH, nicotinamide hypoxanthine dinucleotide phosphate reduced form; $NHXDP^+$, nicotinamide hypoxanthine dinucleotide phosphate; thio-NADPH, thionicotinamide adenine dinucleotide phosphate reduced form; thio-$NADP^+$, thionicotinamide adenine dinucleotide phosphate; UDP, uridine 5′-diphosphate; UNAG, uridine diphospho-*N*-acetylglucosamine; UNAGEP, uridine diphospho-*N*-acetylglucosamine enolpyruvate; UNAM, uridine diphospho-*N*-acetylmuramic acid; 3′-NADPH, β-nicotinamide adenine dinucleotide 3′-phosphate reduced form; 3′-$NADP^+$, β-nicotinamide adenine dinucleotide 3′-phosphate.

0006-2960/95/0434-5390$09.00/0

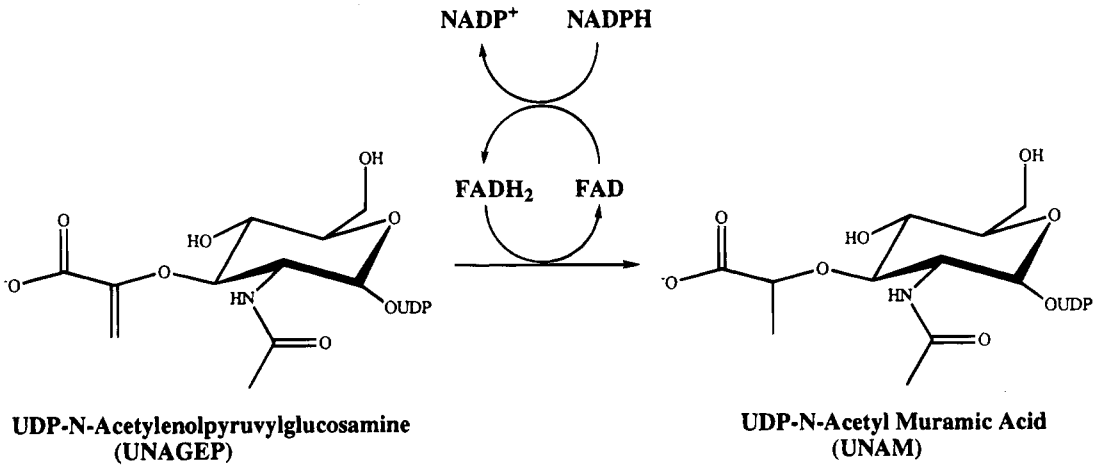

FIGURE 1: Reaction catalyzed by UDP-*N*-acetylenolpyruvylglucosamine reductase.

enzymes and to generate substrates for more detailed analysis of the reactions. In particular, the *Escherichia coli* MurB gene encoding UDP-*N*-acetylenolpyruvylglucosamine reductase has been cloned, sequenced (Pucci et al., 1992), and overexpressed in *E. coli* (Benson et al., 1993). Purification and analysis of the recombinant protein have shown that it contains tightly bound FAD and that it has a M_r in agreement with the DNA sequence predicted M_r of 37 854 (Benson et al., 1993). These results have resolved uncertainties about the requirement for FAD and the molecular size of the intact enzyme (Anwar & Vlaovic, 1979; Taku et al., 1970). The demonstration that the enzyme contains bound flavin has also provided a starting point for explaining the chemical mechanism.

On the basis of NMR studies of deuterium labeled reaction products, the chemical mechanism has been rationalized as an initial NADPH dependent reduction of FAD followed by a direct hydride transfer from $FADH_2$ to the vinylic carbon of UNAGEP (Benson et al., 1993). Delivery of the hydride has been proposed to generate a carbanionic transition state or intermediate that would ultimately be protonated by a solvent equilibrated proton (Benson et al., 1993). One earlier proposal suggested direct transfer of [^{3}H] from 1,4 [4-^{3}H]-NADPH to UNAGEP (Anwar & Vlaovic, 1979).

In contrast to the chemical mechanism, the kinetic mechanism of UDP-*N*-acetylenolpyruvylglucosamine reductase has not been studied in any detail. Substrate saturation curves have been assumed to be hyperbolic (Anwar & Vlaovic, 1979; Benson et al., 1993). Michaelis constants for affinity purified enzyme from wild type *E. coli* have been reported to be $K_{m,NADPH} = 4.6\ \mu M$ and $K_{m,UNAGEP} = 6.5\ \mu M$ (Anwar & Vlaovic, 1979), and for recombinantly produced enzyme have been reported to be $K_{m,NADPH} = 19.9\ \mu M$ and $K_{m,UNAGEP} = 12.5\ \mu M$ (Benson et al., 1993). Also, the enzyme has been shown to be stimulated by monovalent cations (Taku & Anwar, 1973). In particular, stimulation by K^+ has been proposed to involve stabilization of UNAGEP–protein interactions. However, there have been no further detailed reports on the kinetic mechanism of the enzyme.

The availability of purified enzyme has led to successful crystallization of native and heavy atom derivatives of the enzyme (Benson et al., 1994). Future solution of the crystal structure will provide a model for rationalizing the chemical steps in the enol ether reduction. In conjunction with this, a complete description of the microscopic rate constants would provide a basis for thermodynamic analysis of the chemical steps and would lead to an understanding of how the enzyme achieves its catalytic rate enhancement.

As a first step toward a complete kinetic mechanism, we have determined the initial velocity patterns as a function of both substrates. In this study, both the MurA and MurB genes were expressed as fusion constructs with maltose binding protein in order to facilitate rapid purification of the enzymes and to facilitate gram quantity synthesis of substrates and products. The reductase was proteolytically separated from the maltose binding protein/UDP-*N*-acetylenolpyruvylglucosamine reductase fusion protein and then was purified to apparent homogeneity. Purified reductase was used to characterize the steady-state initial velocity patterns of the reaction, and to determine the inhibition constants of reaction products.

MATERIALS AND METHODS

Reagents. Factor Xa, amylose affinity resin, and the pMal-2 cloning system were from New England BioLabs. The Resource Q column was from Pharmacia. The Hi-Pore 318 reverse phase column and the protein dye binding assay were from Bio-Rad. Pefabloc protease inhibitor, catalase, and IPTG were from Boehringer Mannheim. Maltose, triethylammonium bicarbonate, glucose oxidase, β-D-(+)-glucose, UNAG, UDP, 3′-NADPH, 3′-NADP$^+$, thio-NADPH, thio-NADP$^+$, APADPH, APADP$^+$, NEthDPH, NEthDP$^+$, NHXDPH, NHXDP$^+$, α-NADPH, α-NADP$^+$, ADP, and ADP-ribose were from Sigma. Minigels were from Novex.

Cloning and Expression. The MurA gene coding for UDP-*N*-acetylglucosamine enolpyruvyl transferase (Marquardt et al., 1992) and the MurB gene coding for UDP-*N*-acetylenolpyruvylglucosamine reductase (Pucci et al., 1992) were expressed as separate fusion constructs in tandem with the gene for maltose binding protein. Each gene was separately cloned into the pMal-c2 vector, and the vectors were used to transform *E. coli* strain JM109. The cells were maintained on LB agar in 50 μg/mL ampicillin. Cells from a single colony were grown in 10 mL overnight cultures, and the cultures were expanded in 0.5 L of media in 2 L Erlenmeyers to an optical density of 0.8 at 600 nm. At this

density, the cells were induced with 300 μM ITPG. Cells were harvested after 2 h and suspended in 50 mL of 20 mM Tris-HCl, pH 8.0, and 1 mM pefabloc. The cell suspension then was stored at −20 °C.

Purification of UDP-N-Acetylenolpyruvylglucosamine Reductase. Cell paste from 4 L of cell growth was thawed and diluted to a volume of 200 mL in lysis buffer containing 20 mM Tris, pH 8.0, and 200 mM KCl. The cells were lysed by sonication in a sonication horn using a Branson Sonifier 450 for eighteen 1-min cycles at 50% power with 1-min intervals between sonication cycles. The resulting lysate was clarified by centrifugation at 10000*g* for 30 min at 4 °C.

The supernatant was collected and passed over a 5 cm × 10 cm column containing 200 mL of amylose resin equilibrated in lysis buffer. After washing the column with 200 mL of lysis buffer, the bound fusion protein was clearly visible as a yellow band on the column. The fusion protein then was eluted with 100 mL of lysis buffer containing 10 mM maltose. Fractions containing fusion protein were pooled to give 150 mL of 2.6 mg/mL protein. Purified fusion protein was concentrated to 25 mL in an Amicon ultrafiltration cell using a YM30 filter under nitrogen pressure. Factor Xa protease was added to a final ratio of 0.5 mg/390 mg of fusion protein, and the protein solution was dialyzed against three 1 L changes of 50 mM Bis-Tris propane, pH 8.0. Cleavage of maltose binding protein from UDP-*N*-acetylenolpyruvylglucosamine reductase was allowed to proceed for 6 days at 4 °C. After 6 days, cleavage of the fusion protein was judged to be complete by SDS-PAGE on 4−20% gradient minigels.

Maltose binding protein was separated from UDP-*N*-acetylenolpyruvylglucosamine reductase by anion exchange chromatography on a 6 mL Pharmacia Resource Q column. Automated separations were performed on a BioCAD liquid chromatography system. The column was equilibrated in 20 mM Bis-Tris propane and 20 mM Tris, pH 8.0, and injections of ≈50 mg of fusion digest were made. Maltose binding protein and UDP-*N*-acetylenolpyruvylglucosamine reductase were quantitatively separated and eluted in a gradient of NaCl running from 0 to 500 mM over 12 min at a flow rate of 5 mL/min. The yield of fusion protein from the expression system was 390 mg/4 L of cells. Approximately 100 mg of homogeneous UDP-*N*-acetylenolpyruvylglucosamine reductase was recovered after digestion of the fusion and anion exchange chromatography. Enzyme from the anion exchange column was dialyzed against 50 mM Bis-Tris propane, pH 8.0, and was stored in 20% glycerol at −20 °C. The highest specific activity of purified enzyme from several purifications was ≈70 units/mg at 37 °C.

In separate experiments, wild type enzyme was purified from the expressed MurB gene without the maltose binding protein fusion. The K_ms for the wild type enzyme without the 4 amino acid N-terminal extension were similar to the K_ms for the enzyme purified from the fusion protein construct (Falk, 1994). Therefore, enzyme from the fusion protein construct is representative of pure wild type enzyme.

Purification of UDP-N-Acetylglucosamine Enolpyruvyl Transferase. Purification of the MurA gene product, UDP-*N*-acetylglucosamine enolpyruvyl transferase, was identical to the purification of UDP-*N*-acetylenolpyruvylglucosamine reductase up through the affinity step on amylose resin. At this point, purified transferase fusion protein was stored at −80 °C in 20% glycerol. The transferase was used for synthetic reactions as an intact fusion protein, and no digestion to remove maltose binding protein was performed.

Synthesis and Purification of UDP-N-Acetylenolpyruvylglucosamine. Substrate for UDP-*N*-acetylenolpyruvylglucosamine reductase was prepared by enzymatic conversion of UNAG to UNAGEP in the presence of phosphoenolpyruvate and UDP-*N*-acetylglucosamine enolpyruvyl transferase fusion protein. Reactions contained, in a total volume of 200 mL, 50 mM Tris, pH 7.5, 20 mM KCl, 5 mM dithiothreitol, 5 mM UNAG, 5 mM phosphoenolpyruvate, and 2 mg of transferase fusion protein. The reaction was allowed to proceed for 48 h at 37 °C. Products were separated from reactants by anion exchange chromatography on a 6 mL Pharmacia Resource Q column. The column was equilibrated with 10 mM triethylammonium bicarbonate buffer, and 5 mL aliquots of the reaction were injected onto the column. The column was washed with 10 mL of buffer and then was eluted at 5 mL/min with a gradient running from 10 to 300 mM triethylammonium bicarbonate over 30 min. Reaction products were separated in base-line resolution, and UNAGEP eluted at 15 min. Aliquots of purified UNAGEP were pooled and lyophilized. The lyophilized material was dissolved in 100 mL of water and was relyophilized three times to remove buffer salts. The purified material finally was dissolved in 10 mL of water and was stored at 4 °C. The electrospray mass spectrum gave a molecular weight of 677. Solutions of UNAGEP were quantitated by measuring the absorbance at 262 nm and using an extinction coefficient of ϵ_{262} = 10 100 for UDP.

Synthesis and Purification of UDP-N-Acetylmuramic Acid. The product of the UDP-*N*-acetylenolpyruvylglucosamine reductase reaction was prepared by a two step coupled enzymatic conversion of UNAG to UNAM. Reactions contained, in a total volume of 80 mL, 100 mM Tris, pH 8.0, 0.5 mM dithiothreitol, 20 mM UNAG, 30 mM NADPH, 30 mM phosphoenolpyruvate, 10 mg of transferase fusion protein, and 1.2 mg of reductase. The reaction was allowed to proceed at 25 °C and was 90% complete after 42 h. Enzymes were removed by ultrafiltration, and products were separated from reactants by chromatography on a 250 mm × 21.5 mm Hi-Pore 318 reverse phase column. The column was equilibrated with 50 mM ammonium formate, pH 3.3, and 0.3 mL aliquots of the reaction were injected onto the column. The column was eluted isocratically with the same buffer at 10 mL/min. Reaction products were separated in base-line resolution, and UNAM eluted at 13.5 min. Aliquots of purified UNAM were pooled and lyophilized. The lyophilized material was dissolved in 1 L of water and was relyophilized three times to remove buffer salts. The purified material finally was dissolved in 10 mL of water and was stored at 4 °C. The negative ion mass spectrum gave a molecular weight of 679. Solutions of UNAM were quantitated by measuring the absorbance at 262 nm and using an extinction coefficient of ϵ_{262} = 10 100 for UDP.

Enzyme Assay. The standard enzyme assay used to monitor the purification and the activity of stored samples contained, in a final volume of 1 mL, 50 mM Bis-Tris propane, pH 8.0, 50 mM KCl, 125 μM UNAGEP, 150 μM NADPH, and 1 μg of UDP-*N*-acetylenolpyruvylglucosamine reductase. Reaction mixtures without NADPH and enzyme were equilibrated at 37 °C for 10 min. Reactions then were

started by sequential addition of NADPH and enzyme. The decrease in NADPH absorbance at 340 nm was monitored on a Cary 3E, where activities were determined from the linear part of the progress curve within the first 30 s after addition of enzyme. The slope of the initial linear portion of the curve was calculated by linear least squares analysis. Additional assays were performed on a Hewlett Packard 8452A diode array spectrophotometer running the OLIS operating system (OLIS, Bogart, GA). Activities measured on the diode array were calculated from the linear part of the progress curve between 8 and 16 s after addition of enzyme. All assays were performed at 37 °C. An extinction coefficient of 6220 cm^{-1} M^{-1} for NADPH absorbance at 340 nm was used to calculate the specific activity of the enzyme. One unit of activity corresponds to 1 μmol of NADPH consumed/min. Assays at high concentrations of NADPH or NADPH analogs were performed in 0.2 cm path length cells. Protein concentrations were determined by the dye binding assay from Bio-Rad using bovine serum albumin as standard. For the determinations of kinetic parameters and inhibition constants, the reaction conditions were the same as those described above except that the concentrations of NADPH, UNAGEP, and inhibitors were varied as described in the footnotes and legends to the tables and figures. For assays at different pH values, 50 mM Bis-Tris propane was adjusted to the specific pH with HCl. A molecular weight of 38 334, based on the sum of the enzyme polypeptide and four amino acid (ISEF) N-terminal linker, was used for conversion of protein concentrations to molar units.

Anaerobic Exchange Reaction. Anaerobic exchange reactions contained, in a final volume of 2 mL, 50 mM Bis-Tris propane, pH 8.0, 50 mM KCl, 50 μM NADPH, 100 mM β-D-(+)-glucose, 100 units of glucose oxidase, 100 units of catalase, and varied amounts of thio-$NADP^+$. Reaction mixtures were added to a Thunberg type cuvette, and the cuvette was connected to an argon/vacuum gas train through a glass stopcock. The sample was maintained at 37 °C for 30 min and was alternately purged and flooded with argon at least 10 times. Sealed cuvettes under an argon atmosphere then were transferred to a Hewlett Packard 8452A diode array spectrophotometer. Aerobic enzyme was drawn into a 25 μL gas tight Hamilton syringe, and reactions were started by injection of enzyme through a septum at the top of the cuvette. The final concentration of enzyme was 50 μg/mL (1.3 μM). Under these conditions, with the high concentration of glucose and glucose oxidase, the enzyme volume was small enough that any oxygen added to the system was scavenged immediately and made no difference in the final rates. The rate of thio-NADPH production at 37 °C was measured at 396 nm and was linear for at least 5 min. The initial exchange rate was calculated from the first 3 min using an extinction coefficient of $\epsilon_{396} = 11\,300$.

Data Analysis. Kinetic parameters were determined by nonlinear regression analysis in the program KinetAsyst or were determined by the nonlinear regression algorithm in SigmaPlot from Jandel Scientific. Substrate saturation curves were fitted to eqs 1 and 2, inhibition data were fitted to eqs 3−7, and mechanism data were fitted to eq 8. Double inhibition data were fitted to eq 9 (Cleland, 1990). In cases where the inhibition data could be fitted to more than one model, the simplest model with the lowest χ^2 is reported in Table 5.

$$v = (V_m S)/(K_m + S) \quad (1)$$

$$v = (V_m S)/(K_m + S + (S^2/K_i)) \quad (2)$$

$$v = (V_m S)/(K_m(1 + (I/K_{is})) + S) \quad (3)$$

$$v = (V_m S)/(K_m + S(1 + (I/K_{ii}))) \quad (4)$$

$$v = (V_m S)/(K_m + S(1 + (I/K_{ii})) + (S^2/K_i)) \quad (5)$$

$$v = (V_m S)/(K_m(1 + (I/K_{is})) + S(1 + (I/K_{ii}))) \quad (6)$$

$$v = (V_m S)/(K_m(1 + (I/K_{is})) + S(1 + (I/K_{ii})) + (S^2/K_i)) \quad (7)$$

$$v = (V_m AB)/(K_{ma}B(1 + (B/K_{ib})) + K_{mb}A(1 + (A/K_{ia})) + AB) \quad (8)$$

$$1/v = (1/v_0)[1 + I/K_i + J/K_j + IJ/(\beta K_i K_j)] \quad (9)$$

RESULTS

Purification of UDP-N-Acetylenolpyruvylglucosamine Reductase. The commercially available pMal-2 cloning vector was used to construct a high expression level clone of UDP-*N*-acetylenolpyruvylglucosamine reductase fused to the C-terminus of maltose binding protein. The fusion construct was expressed in JM109 cells to a level of ≈100 mg/L of cell growth and was purified rapidly from cell extracts in a single step by affinity chromatography on amylose. Subsequent proteolysis and anion exchange chromatography yielded essentially homogeneous UDP-*N*-acetylenolpyruvylglucosamine reductase, as shown in Figure 2. Electrospray mass spectrometry of the recombinant protein gave a mass of 38 344 Da, which agrees closely with the expected mass based on the sum of the cDNA encoded polypeptide (Pucci et al., 1992) and the four amino acid linker peptide remaining after proteolysis of the fusion. Purified enzyme contained tightly bound FAD and was fully active as purified. Addition of FAD to the purified protein had no effect on activity. The spectrum of bound FAD exhibited absorption maxima at 273, 360, and 463 nm and a pronounced shoulder at 492 nm. The A_{280}/A_{463} ratio was 7.8. Bound FAD was released from the enzyme in 8 M guanidine hydrochloride and was quantitated optically based on $\epsilon_{450} = 11\,300$. The ratio of FAD/protein was 1, where the protein concentration was determined by the Coomassie dye binding assay. Enzyme was optimally active at pH 8.0.

Monovalent Cation Activation. Previous studies of UDP-*N*-acetylenolpyruvylglucosamine reductase from *Enterobacter cloacae* have shown that monovalent cations stimulate reductase activity (Taku & Anwar, 1973). The same experiments were performed here to determine the optimal conditions for activity of recombinant *E. coli* enzyme, and the results were qualitatively very similar. Activity of UDP-*N*-acetylenolpyruvylglucosamine reductase was stimulated by K^+, NH_4^+, Rb^+, Na^+, and Cs^+. In the absence of monovalent cations, only minimal enzyme activity was observed in comparison to controls without enzyme. Divalent cations, including 20 mM Mg^{2+}, 20 mM Mn^{2+}, 20 mM Co^{2+}, and 20 mM Zn^{2+}, had no activating effect on the enzyme.

Monovalent cations demonstrated hyperbolic saturable activation over the range of 0−100 mM. The enzyme was

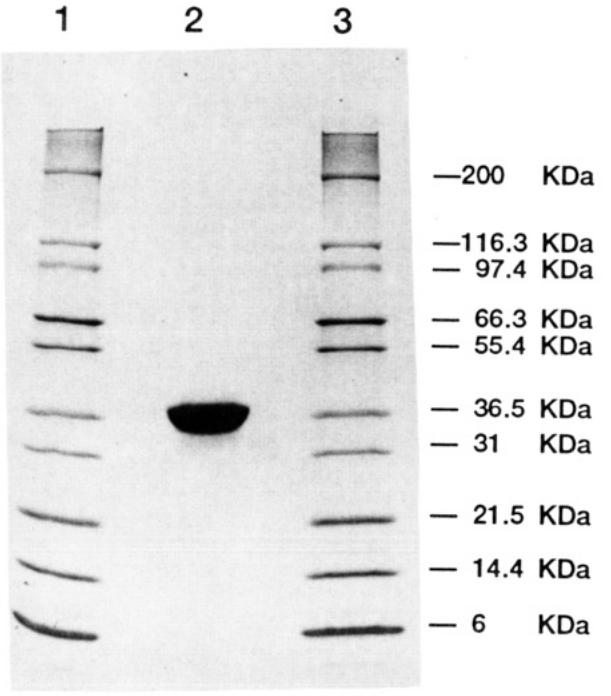

FIGURE 2: Analysis of purified UDP-*N*-acetylenolpyruvylglucosamine reductase by SDS−PAGE. Enzyme was purified as described under Materials and Methods and was subjected to electrophoresis on a 4−20% reducing SDS gel. Lanes 1 and 3 contained molecular weight markers, and lane 2 contained 25 μg of enzyme.

maximally activated by K^+ in the range of 30−50 mM. A small degree of activation was provided by Na^+ and Cs^+. The activation curves at pH 8.0 for each cation were fitted to eq 1 to obtain an activation constant, K_A, and Table 1 lists these values. The K_As were in the range of 2−12 mM, except for Na^+, which was 25 mM. The maximal activities at saturating cation concentrations were K^+ = 50 units/mg, NH_4^+ = 35 units/mg, Rb^+ = 33 units/mg, Na^+ = 5 units/mg, and Cs^+ = 2 units/mg.

The K_ms for each substrate then were determined at 2 and 50 mM, or at 2 and 100 mM concentrations of each monovalent cation. Saturation curves for NADPH and UNAGEP were fitted to eq 1. In cases where substrate inhibition was observed, these data were fitted to eq 2. The weakest activators, Na^+ and Cs^+, yielded the highest K_ms for both NADPH and UNAGEP, and the activities were too low to measure at 2 mM cation. The three strongest activators, K^+, NH_4^+, and Rb^+, gave very similar K_ms for UNAGEP, which ranged from 13 to 20 μM, at high cation concentrations (50 or 100 mM). At low cation concentrations (2 mM K^+, NH_4^+, and Rb^+), the K_ms for UNAGEP increased approximately 2-fold, and the k_{cat}s all decreased. At high K^+, NH_4^+, and Rb^+ concentrations (50 or 100 mM), the K_ms for NADPH varied more significantly, from 12 to 45 μM. At 2 mM K^+ and Rb^+, the K_ms for NADPH increased approximately 2-fold, and the k_{cat}s decreased. The one exception was 2 mM NH_4^+, where the K_m for NADPH decreased as compared to 100 mM NH_4^+.

Substrate Inhibition. Initial experiments to measure K_ms for UNAGEP gave poor fits to eq 1 and suggested the possibility of substrate inhibition. Consequently, several UNAGEP saturation curves were obtained at pH 6.0, 7.0, and 8.0. Extensive substrate inhibition was observed at pH 6.0, and significant inhibition also was observed at pH 7.0 and 8.0, as shown in Figure 3. All the UNAGEP saturation curves were obtained at 150 μM NADPH, which was saturating at pH 7.0 and 8.0. At pH 6.0, an additional saturation curve was obtained at 400 μM NADPH to assure saturation by NADPH (results not shown). These data also demonstrated substantial UNAGEP substrate inhibition, which indicates that the greater extent of inhibition at pH 6.0 is due to ionizations at pH 6.0 and not due to subsaturating cofactor concentrations. Also, at pH 8.0, the measurements were performed at up to 100 times K_m for UNAGEP, and there was no indication of a plateau in substrate inhibition, which indicates complete substrate inhibition rather than partial inhibition.

In contrast, most saturation curves for NADPH could be fitted to eq 1. However, at very low UNAGEP concentrations, NADPH saturation curves sometimes were better described by eq 2. The shape of the curves was pH dependent, as shown in Figure 3. At pH 6.0, NADPH saturation profiles were well described by eq 1, but at pH 7.0 and 8.0 the data were best described by eq 2. Consequently, all UNAGEP curves were fitted to eq 2, and NADPH curves were fitted to eqs 1 or 2.

Table 1: Kinetic Constants for Enzyme Activation by Monovalent Cations

			UNAGEP[a]			NADPH[b]			
cation	ionic radius (Å)	[cation] (mM)	$K_{m,UNAGEP}$ (μM)	k_{cat} (s^{-1})	$K_{i,UNAGEP}$ (μM)	$K_{m,NADPH}$ (μM)	k_{cat} (s^{-1})	$K_{i,NADPH}$ (μM)	K_A[c] (mM)
K^+	1.33	50	20 ± 1	57 ± 3	330 ± 40	22 ± 1	36 ± 1		5.3 ± 0.7
		2	46 ± 6	16 ± 1	400 ± 80	43 ± 8	14 ± 1	580 ± 180	
NH_4^+	1.43	100	13 ± 2	35 ± 3	500 ± 130	45 ± 1	16 ± 1		3.0 ± 0.2
		2	27 ± 1	10 ± 1		28 ± 4	12 ± 1	650 ± 140	
Rb^+	1.47	100	17 ± 1	26 ± 1		12 ± 1	26 ± 1		12 ± 2
		2	34 ± 1	4.9 ± 0.1		21 ± 4	4.8 ± 0.4	790 ± 290	
Na^+	0.97	100	42 ± 5	4.8 ± 0.3		62 ± 10	4.0 ± 0.3		25 ± 12
Cs^+	1.67	100	350 ± 50	2.6 ± 0.2	2100 ± 500	170 ± 20	1.0 ± 0.1		2.0 ± 1.4

[a] For K^+, Rb^+, Na^+, and NH_4^+, the UNAGEP concentrations were varied from 0 to 200 μM with NADPH fixed at 150 μM. For Cs^+, the UNAGEP concentrations were varied from 0 to 1000 μM with NADPH fixed at 1000 μM. Saturation profiles were fitted to either eq 1 or 2. All assays were performed at 37 °C as described under Materials and Methods. [b] For K^+, Rb^+, and NH_4^+, the NADPH concentrations were varied from 0 to 200 μM with UNAGEP fixed at 125 μM. For Na^+, the NADPH concentrations were varied from 0 to 300 μM with UNAGEP fixed at 125 μM. For Cs^+, the NADPH concentrations were varied from 0 to 1500 μM with UNAGEP fixed at 2500 μM. Saturation profiles were fitted to either eq 1 or 2. All assays were performed at 37 °C as described under Materials and Methods. [c] Saturation profiles as a function of varied cation were fitted to eq 1 to obtain K_As for each monovalent cation at pH 8.0. The concentrations of UNAGEP and NADPH were 125 and 150 μM, respectively.

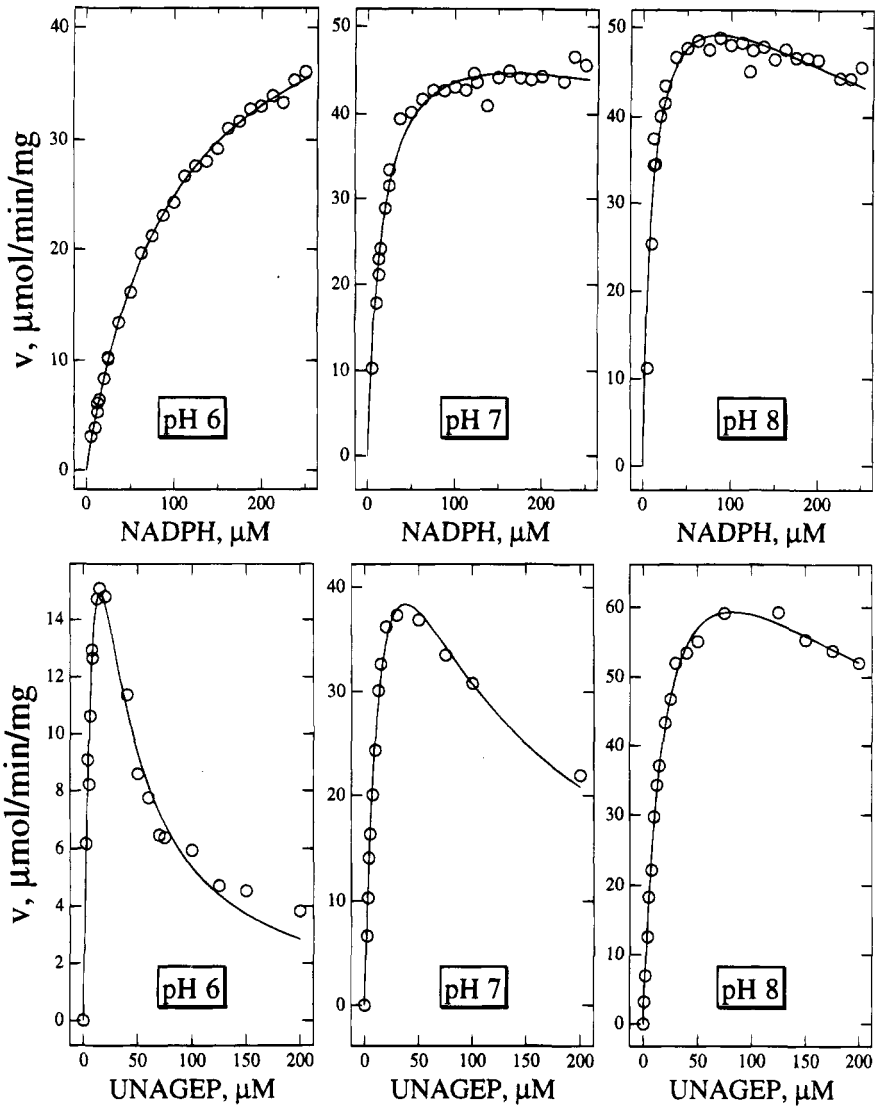

FIGURE 3: Substrate inhibition by NADPH and UNAGEP at pH 6.0, 7.0, and 8.0. Enzyme was assayed as described under Materials and Methods as a function of either NADPH or UNAGEP concentration. The top three panels show the saturation profiles for NADPH at a fixed concentration of 15 μM UNAGEP. The bottom three panels show the saturation profiles for UNAGEP at a fixed concentration of 150 μM NADPH. The lines through the data were all obtained by fitting to eq 2, except for the line through the NADPH data at pH 6.0, which was obtained by fitting to eq 1.

Table 2: Kinetic Constants for Substrate Inhibition

	UNAGEP[a]			NADPH[b]		
pH	$K_{m,UNAGEP}$ (μM)	k_{cat} (s^{-1})	$K_{i,UNAGEP}$ (μM)	$K_{m,app,NADPH}$ (μM)	k_{cat} (s^{-1})	$K_{i,NADPH}$ (μM)
pH 6.0	25 ± 10	40 ± 12	10 ± 3	100 ± 4	32 ± 1	
pH 7.0	18 ± 2	48 ± 3	81 ± 11	17 ± 2	35 ± 1	1600 ± 580
pH 8.0	20 ± 1	57 ± 3	330 ± 40	11 ± 2	40 ± 2	660 ± 130

[a] For substrate inhibition profiles by UNAGEP in Figure 3, assays were performed as described under Materials and Methods with the NADPH concentration fixed at 150 μM. Data were fitted to eq 2. [b] For substrate inhibition profiles by NADPH in Figure 3, assays were performed as described under Materials and Methods with the UNAGEP concentration fixed at 15 μM. Data were fitted to eq 1 for the pH 6.0 data, and to eq 2 for the pH 7.0 and 8.0 data. The reported K_ms are apparent values because the UNAGEP concentration was subsaturating in each experiment.

Table 2 provides the kinetic constants for the saturation profiles in Figure 3. The K_is for UNAGEP were 10 μM, 81 μM, and 330 μM at pH 6.0, 7.0, and 8.0, which illustrates the fact that UNAGEP substrate inhibition was weaker at more basic pH values. In comparison, the K_is for NADPH were very high, where K_i = 1600 μM at pH 7.0 and K_i = 660 μM at pH 8.0, and the k_{cat}s were similar at pH 6.0, 7.0, and 8.0.

Alternate Dinucleotides as Substrates for UDP-N-Acetylenolpyruvylglucosamine Reductase. Several dinucleotides were tested as possible alternate substrates of UDP-*N*-acetylenolpyruvylglucosamine reductase, and several other than NADPH actively reduced the enzyme. Table 3 lists the dinucleotides capable of catalytic reduction of the enzyme. All of the 2′- or 3′-phosphorylated dinucleotide analogs were substrates, except for thio-NADPH. The

Table 3: Kinetic Constants for Analogs of NADPH as Alternate Substrates[a]

substrate	ϵ'_0 (mV)	K_m (μM)	k_{cat} (s^{-1})	λ_{max} (nm)	ϵ at λ_{max} ($cm^{-1}\,M^{-1}$)
NADPH	−320	22 ± 1	36 ± 1	340	6220
NHXDPH	−320	47 ± 2	36 ± 1	340	6220
3′-NADPH	−320	250 ± 50	49 ± 6	340	6220
α-NADPH	−320	780 ± 120	42 ± 3	340	6220
thio-NADPH	−285			395	11300
NADH	−320			340	6220

[a] Enzyme assays were performed as described under Materials and Methods at 37 °C. Analogs of NADPH were varied from 0 to 200 μM (NHXDPH), 0 to 250 μM (3′-NADPH), and 0 to 2000 μM (α-NADPH), at a fixed UNAGEP concentration of 125 μM. Data were fitted to eq 1. Blanks indicate that there was no detectable turnover of the reductant under the standard assay conditions.

nonphosphorylated dinucleotide NADH was not a substrate. The hypoxanthine analog was a reasonable substrate with a relatively low K_m of 47 μM, whereas the 3′-NADPH and α-NADPH were much poorer substrates with K_ms of 250 μM and 780 μM, respectively.

Steady-State Initial Velocity Patterns as a Function of NADPH and UNAGEP at pH 8.0. Initial velocity patterns were obtained by varying the NADPH concentration at several fixed concentrations of UNAGEP, and by varying the UNAGEP concentration at several fixed NADPH concentrations. For the purpose of obtaining diagnostic reciprocal plots, several sets of data were obtained at varied substrate concentrations at K_m and above. Figure 4 illustrates the results of these experiments.

At low UNAGEP concentrations between 12 and 20 μM, the reciprocal plots as a function of NADPH displayed a slight curvature due to substrate inhibition by NADPH. By comparison, at 40 μM UNAGEP and above, the reciprocal plots were linear. This pattern also changed from parallel between 12 and 20 μM UNAGEP to intersecting at concentrations of 80 μM and above. Moreover, the $1/v$ intercepts decreased at each UNAGEP concentration up to ≈40 μM, and thereafter, the intercepts were constant and the slopes began to increase. This inflection in the slope values represents competitive substrate inhibition by UNAGEP.

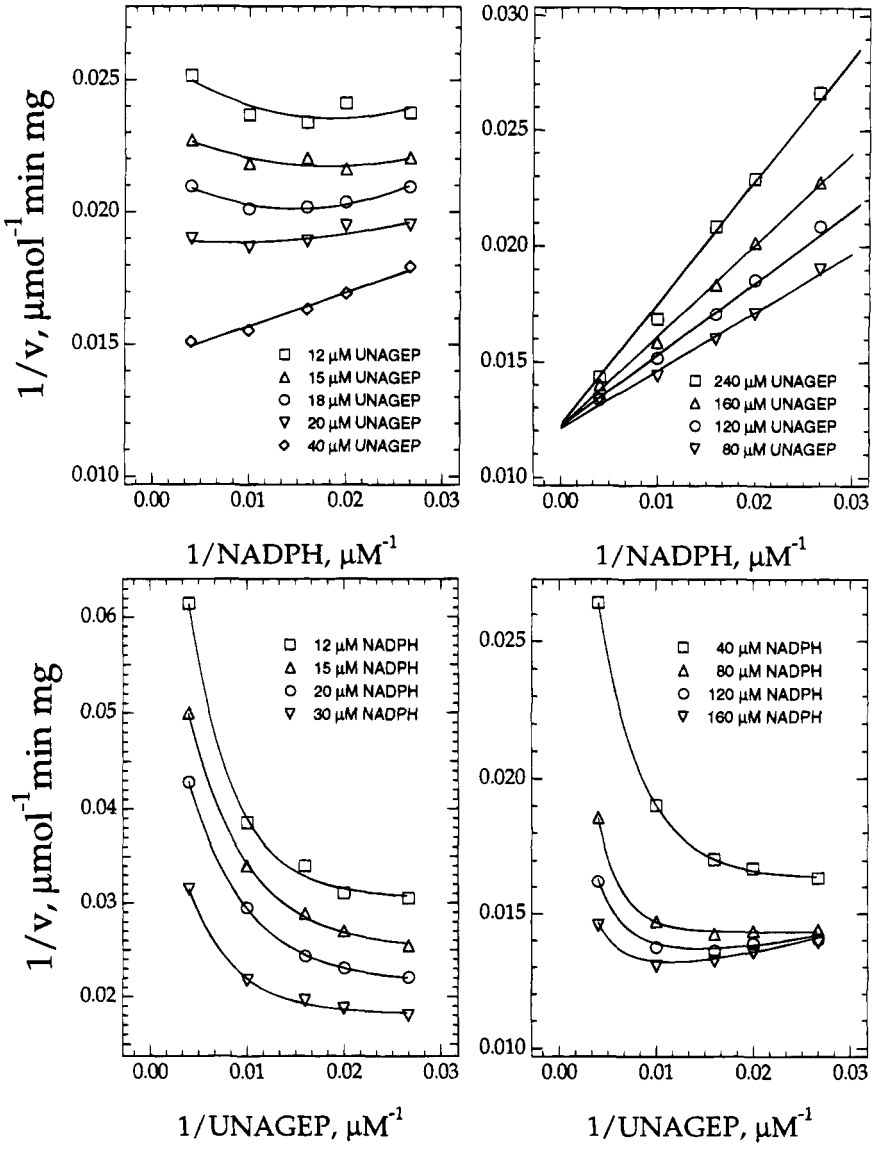

FIGURE 4: Initial velocity patterns as a function of varied NADPH and UNAGEP. Enzyme was assayed as described under Materials and Methods as a function of either NADPH concentration at several fixed UNAGEP concentrations, or as a function of UNAGEP concentration at several fixed NADPH concentrations. Concentrations on the $1/S$ axis were chosen to emphasize the pattern of convergence on the $1/v$ axis. The lines through the data represent fits to either eq 1 or eq 2.

Table 4: Kinetic Constants for Ping Pong Bi Bi Mechanism with Double Substrate Inhibition[a]

pH	$K_{m,UNAGEP}$ (μM)	$K_{i,UNAGEP}$ (μM)	$K_{m,NADPH}$ (μM)	$K_{i,NADPH}$ (μM)	k_{cat} (s^{-1})
7.0	19 ± 3	8 ± 2	17 ± 4	250 ± 60	51 ± 5
8.0	24 ± 3	73 ± 19	17 ± 3	910 ± 670	62 ± 3
9.0	42 ± 3	430 ± 140	20 ± 3	490 ± 120	41 ± 1

[a] Enzyme assays were performed as described under Materials and Methods at 37 °C. At each pH, a square matrix of 64 enzyme velocities was obtained, and the pooled data were fitted to eq 8. In order to obtain each square matrix, saturation curves were obtained at eight concentrations of UNAGEP with NADPH fixed at each of the same eight concentrations. The concentrations used were 10, 20, 30, 50, 75, 100, 150, and 200 μM at pH 8. For pH 7 and 9 the concentrations were 7, 16, 22, 37, 73, 110, 183, and 244 μM.

The reciprocal plots of varied UNAGEP at fixed NADPH concentrations all demonstrated significant substrate inhibition by UNAGEP. The plots were also parallel between 12 and 30 μM NADPH. At the highest NADPH concentrations, between 80 and 160 μM, the plots still demonstrated UNAGEP substrate inhibition, but began to change slope. However, there was no inflection point where the intercepts became constant and the slopes continued to increase. At NADPH concentrations above 160 μM, the reciprocal plots were all essentially superimposable (data not shown). These data demonstrate that the effect of NADPH was saturating at $\approx$160 μM and that NADPH was not an effective competitive inhibitor against UNAGEP at high UNAGEP concentrations.

The patterns in Figure 4 provide diagnostic evidence of a ping pong bi bi kinetic mechanism with double competitive substrate inhibition (Segel, 1975). In this case, UNAGEP is a strong competitive substrate inhibitor, whereas NADPH is a relatively weak competitive substrate inhibitor. Based on these initial velocity patterns, a complete matrix of 64 velocities at eight varied NADPH and eight varied UNAGEP concentrations, including values above and below the K_ms, was obtained at pH 7.0, 8.0, and 9.0.

The initial velocity patterns at each pH were similar to those in Figure 4, except that the degree of substrate inhibition varied as a function of pH. Thus, the kinetic mechanism was the same between pH 7.0 and 9.0. The dataset at each pH was fitted to eq 8 to obtain the kinetic constants. Table 4 lists the constants from these fits. The K_ms for NADPH were relatively unchanged from pH 7.0 to 9.0, whereas the K_ms for UNAGEP increased at more basic pH values. The K_i for UNAGEP inhibition also increased dramatically at more basic pH values, which is in agreement with the data in Figure 3. In contrast, the K_i for NADPH was relatively high at each pH tested. This is consistent with the evidence in Figure 3 that NADPH is a weak substrate inhibitor and that NADPH inhibition is only observable at very low UNAGEP concentrations.

Inhibition by Products, Product Analogs, and Substrate Analogs. Reaction products, product analogs, and substrate analogs were tested as inhibitors of UDP-*N*-acetylenolpyruvylglucosamine reductase to explore the binding requirements of the enzyme. Steady-state assays in the presence of $NADP^+$ demonstrated noncompetitive inhibition with respect to NADPH, as shown in Figure 5. The K_{is} and K_{ii} were 82 μM and 520 μM, respectively. Thus, $NADP^+$ can bind to two forms of the enzyme. The inhibition pattern also was noncompetitive with respect to UNAGEP, with a small amount of substrate inhibition due to UNAGEP. Table 5 provides the inhibition constants for all the reaction products and substrate analogs that were tested.

In contrast, $APADP^+$ was a competitive inhibitor with respect to NADPH, as shown in Table 5. Thus, the change of a $-NH_2$ to a $-CH_3$ on the side chain of the pyridine ring of $NADP^+$ caused the inhibitor to bind to only one form of the enzyme, rather than two forms as with $NADP^+$. In this case, however, the K_{is} increased from 82 μM for $NADP^+$ to 470 μM for $APADP^+$. With respect to UNAGEP, $APADP^+$ was an uncompetitive inhibitor with slight substrate inhibition due to UNAGEP. All other $NADP^+$ analogs tested were noncompetitive inhibitors with respect to NADPH and demonstrated noncompetitive inhibition in addition to substrate inhibition with respect to UNAGEP. The inhibition constants were all in the range of 100−1100 μM.

The product inhibition pattern with fixed UNAM and varied NADPH was uncompetitive with a K_{ii} of 8.4 mM, as shown in Table 5. Attempts were made to obtain the

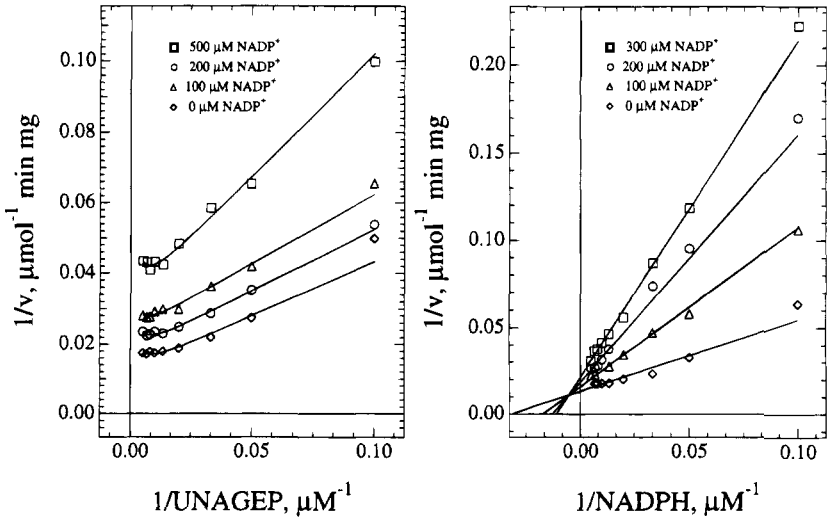

FIGURE 5: Product inhibition by $NADP^+$. Inhibition patterns in the presence of several fixed concentrations of $NADP^+$ were obtained as a function of varied UNAGEP or NADPH. Lines through the data represent fits to eq 7 for UNAGEP and eq 6 for NADPH. Table 5 lists the fitted parameters.

Table 5: Kinetic Constants for Inhibition by Reaction Products, Substrate Analogs, and Product Analogs

	varied NADPH[a]			varied UNAGEP[b]			
inhibitor	type[c]	K_{is}	K_{ii}	type[c]	K_{is}	K_{ii}	K_i (μM)
$NADP^+$	N	82 ± 8 μM	520 ± 100 μM	NSI	570 ± 130 μM	250 ± 20 μM	510 ± 90
$NHXDP^+$	N	120 ± 10 μM	1100 ± 300 μM	NSI	750 ± 220 μM	370 ± 40 μM	560 ± 130
$NEthDP^+$	N	110 ± 10 μM	1070 ± 230 μM	NSI	660 ± 140 μM	380 ± 30 μM	430 ± 90
thio-$NADP^+$	N	190 ± 10 μM	690 ± 80 μM	NSI	270 ± 60 μM	250 ± 60 μM	130 ± 40
3′-$NADP^+$	N	780 ± 50 μM	10 ± 3.9 mM	NSI	3.0 ± 1.2 mM	2.5 ± 0.4 mM	370 ± 70
$APADP^+$	C	470 ± 30 μM		USI		970 ± 150 μM	160 ± 40
ADP	C	5.4 ± 0.4 mM		NSI	25 ± 7 mM	14 ± 2 mM	280 ± 70
ADP-ribose	C	5.1 ± 0.6 mM		NSI	97 ± 72 mM	21 ± 3 mM	310 ± 70
UNAM	U		8.4 ± 1.1 mM	–[d]	–	–	–
UDP	N	14 ± 7 mM	33 ± 5 mM	N	2.8 ± 0.4 mM	49 ± 10 mM	
UNAG	N	41 ± 2 mM	89 ± 13 mM	C	5.7 ± 1 mM		

[a] For inhibition with $NADP^+$, $NHXDP^+$, $NEthDP^+$, thio-$NADP^+$, 3′-$NADP^+$, and $APADP^+$, the NADPH concentration was varied from 0 to 200 μM and the UNAGEP concentration was fixed at 125 μM. For inhibition with ADP, ADP-ribose, UDP, and UDPNAG, the NADPH concentration was varied from 7 to 244 μM and the UNAGEP concentration was fixed at 200 μM. Three or four separate fixed inhibitor concentrations were used in each experiment, and the data were fitted to eqs 3, 4, and 6. [b] For inhibition with $NADP^+$, $NHXDP^+$, $NEthDP^+$, thio-$NADP^+$, 3′-$NADP^+$, and $APADP^+$, the UNAGEP concentration was varied from 0 to 200 μM and the NADPH concentration was fixed at 150 μM. For inhibition with ADP, ADP-ribose, UDP, and UNAG, the UNAGEP concentration was varied from 7 to 244 μM and the NADPH concentration was fixed at 200 μM. Three or four separate fixed inhibitor concentrations were used in each experiment, and the data were fitted to eqs 3, 5, 6, and 7. [c] N = noncompetitive, C = competitive, U = uncompetitive, USI = uncompetitive with substrate inhibition, and NSI = noncompetitive with substrate inhibition. [d] Small amounts of UNAGEP in the UNAM prevented independent variation of the UNAGEP concentration, and therefore the inhibition pattern as a function of UNAGEP could not be determined.

inhibition pattern with fixed UNAM and varied UNAGEP, but the UNAM appeared to contain trace amounts of UNAGEP, and it was not possible to vary the UNAGEP concentration independently. For instance, even though the UNAM was chromatographically pure and pure by electrospray mass spectrometry, at the millimolar concentrations required to observe inhibition, enzyme turnover was observed in the absence of any added UNAGEP. As a result, it was not possible to obtain any velocities below the K_m for UNAGEP, and therefore, the inhibition pattern could not be determined.

Several experiments were performed to determine whether or not nucleotides can bind to the reductase. Thus, ADP, ADP-ribose, UDP, and UNAG were tested as inhibitors. All of these provided measurable inhibition, but at very high concentrations, with inhibition constants in the 5 mM to 97 mM range. In particular, the experiments demonstrated that UNAG is a weak competitive inhibitor with respect to UNAGEP, with a K_{is} of 5.7 mM. At the same pH, UNAGEP has a K_m of 24 μM. The only difference between the two molecules is the enolpyruvyl moiety of UNAGEP. Therefore, the enolpyruvyl moiety provides a 237-fold change in the ratio of rate constants determining K_{is} and K_m.

In general, the high inhibition constants for all the nucleotides suggest that the nucleotide portions of NADPH and UNAGEP only provide a small part of the binding energy of the substrates. Moreover, at subsaturating concentrations of 50 μM NADPH and 50 μM UNAGEP, there was no inhibition at 1 mM by β-NAD or 2′,3′-cyclic $NADP^+$, and therefore, the enzyme requires the free 2′-phosphoryl group of NADPH for binding. Under the same conditions, the enzyme also did not exhibit any inhibition in the presence of 5 mM NAG, NAGP, MA, or NAMA, and thus the *N*-acetylglucosamine portion of the substrate is not able to bind to the enzyme by itself.

Double Inhibition by UNAG and $APADP^+$. The experiments described above identified UNAG and $APADP^+$ as competitive inhibitors with respect to UNAGEP and NADPH. A double inhibition experiment was performed at fixed subsaturating concentrations of UNAGEP and NADPH to determine whether or not the two inhibitors interact with each other on the enzyme's surface (Cleland, 1990). The plot of reciprocal velocities versus $APADP^+$ at three fixed concentrations of UNAG yielded parallel lines, as shown in Figure 6. The data were fitted to eq 9. The fit yielded values of $v_0 = 28 \pm 2\ s^{-1}$, $K_{i,APADP^+} = 770 \pm 60\ \mu M$, $K_{j,UNAG} = 25 \pm 2$ mM, and β approached ∞. The parallel pattern in the Dixon plot indicates that the inhibitors can bind to the same form of the enzyme but are mutually exclusive.

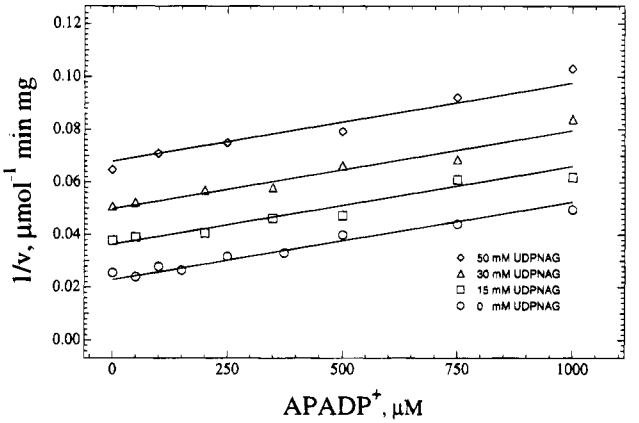

FIGURE 6: Double inhibition by $APADP^+$ and UNAG. The inhibition pattern as a function of varied $APADP^+$ was obtained at three fixed concentrations of UNAG with the concentrations of UNAGEP and NADPH fixed at 50 μM. The lines through the data represent the best fit to eq 9 with $\beta = \infty$.

Anaerobic Exchange Reaction with Thio-$NADP^+$. The ping pong kinetic mechanism predicts product release of $NADP^+$ before binding and reduction of UNAGEP. In order to provide evidence of product release, the enzyme was reacted under anaerobic conditions with NADPH and thio-$NADP^+$ to generate reduced enzyme from NADPH and to look for reoxidation of $FADH_2$ by thio-$NADP^+$. This reaction would provide direct evidence that the reduced enzyme releases product and then binds a second molecule in the NADPH site. Thio-$NADP^+$ was selected as the oxidant because it is isosteric with $NADP^+$ and because the reduced form, thio-NADPH, has a λ_{max} separate from

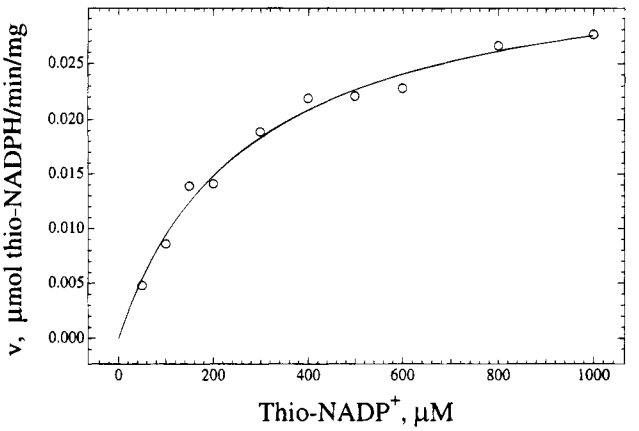

FIGURE 7: Anaerobic exchange reaction with thio-NADP$^+$. Anaerobic enzyme was prepared and assayed for exchange activity as described in the Materials and Methods. The line through the data represents the best fit to eq 1.

NADPH and has a high extinction coefficient of ϵ_{396} = 11 300. Therefore, thio-NADPH production would be directly observable in continuous spectrophotometric assays even in the presence of high NADPH concentrations.

At high enzyme (50 μg/mL) and substrate concentrations (500 μM NADPH, 50−1000 μM thio-NADP$^+$), slow exchange of reduced flavin with thio-NADP$^+$ was observed. The exchange rate was linear for 5−10 min, and the initial rate was saturable at high thio-NADP$^+$ concentrations, as shown in Figure 7. The K_m for thio-NADP$^+$ was 270 ± 30 μM. This is similar to the inhibition constants for thio-NADP$^+$, which were K_{is} = 190 ± 10 μM and K_{ii} = 690 ± 80 μM with NADPH as the varied substrate, and K_{is} = 270 ± 60 μM and K_{ii} = 250 ± 60 μM with UNAGEP as the varied substrate. The anaerobic slow exchange of reduced flavin with thio-NADP$^+$ supports all the other evidence for a ping pong mechanism.

DISCUSSION

Recombinant UDP-*N*-acetylenolpyruvylglucosamine reductase was purified to apparent homogeneity after expression as a fusion with maltose binding protein. Based on the spectrum of the tightly bound flavin, the M_r, the specific activity, and the Michaelis constants, the *E. coli* enzyme purified in these studies appears identical to the recombinant *E. coli* protein recently purified by others (Benson et al., 1993). Expression and purification of the recombinant protein in separate expression systems by separate laboratories now provide substantial evidence that UDP-*N*-acetylenolpyruvylglucosamine reductase is in fact a flavoprotein, in contrast to an earlier study that did not detect the presence of enzyme bound FAD (Anwar & Vlaovic, 1979). Expression as a fusion protein provided the added advantage of simple and rapid purification in high yield. Recombinant enzyme was stable to proteolysis, and no evidence of nonspecific degradation was detected.

Monovalent cation activation of the *E. coli* enzyme was very similar to that observed for enzyme from *E. cloacae* and followed the general specificity observed in numerous other enzymes (Suelter, 1970). The results suggest that monovalent cations with ionic radii in the 1.3−1.5 Å range have the preferred size for activation. At subsaturating cation concentrations, the K_ms in general increased and the k_{cat}s

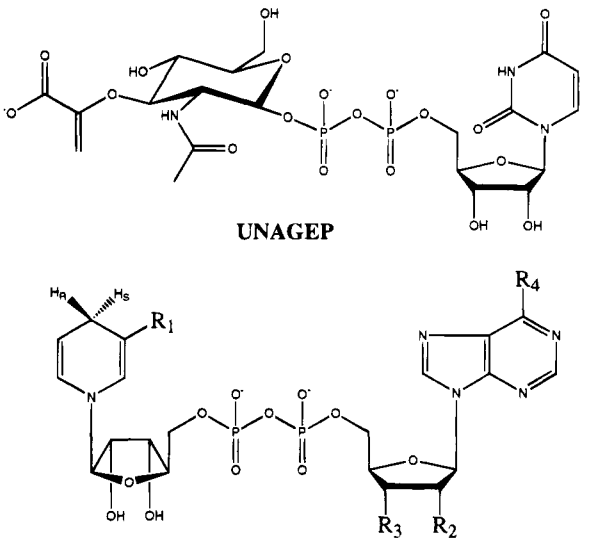

ß-NADPH	R_1 = $CONH_2$	R_2 = PO_4^{2-}	R_3 = OH	R_4 = NH_2
Thio-NADPH	R_1 = $CSNH_2$	R_2 = PO_4^{2-}	R_3 = OH	R_4 = NH_2
APADPH	R_1 = $COCH_3$	R_2 = PO_4^{2-}	R_3 = OH	R_4 = NH_2
3'-NADPH	R_1 = $CONH_2$	R_2 = OH	R_3 = PO_4^{2-}	R_4 = NH_2
NHXDPH	R_1 = $CONH_2$	R_2 = PO_4^{2-}	R_3 = OH	R_4 = OH
2'-3'-cNADPH	R_1 = $CONH_2$	R_2-R_3 = PO_4^{1-}		R_4 = NH_2
ß-NADH	R_1 = $CONH_2$	R_2 = OH	R_3 = OH	R_4 = NH_2

FIGURE 8: Structures of UNAGEP and NADPH.

decreased, as compared to the values at saturating cation concentrations. For this mechanism both K_m and k_{cat} are complex collections of rate constants, and therefore it is not known yet whether the measured effects are specific for binding or catalysis.

Saturation curves for NADPH and UNAGEP provided clear evidence of substrate inhibition as a function of pH. Data in Figure 3 suggest a reciprocal relationship between the two phenomena. At pH 6.0, UNAGEP exhibited extensive inhibition, whereas NADPH showed no substrate inhibition. As the pH became more basic, UNAGEP exhibited less substrate inhibition, whereas substrate inhibition by NADPH became more pronounced. This may suggest that ionizable groups on the enzyme control binding specificity. In the protonated form, the enzyme would prefer UNAGEP, and in the unprotonated form it would have increased affinity for NADPH.

In this regard, the apparent reciprocal pH dependence of substrate inhibition between the two substrates may suggest a common binding determinant. If a single binding site exists, the protonation state may regulate the preference of the site. Alternatively, if two sites exist, they may share an overlapping subsite with ionizable groups involved in binding. Both substrates contain a common ribose diphosphate core, as shown in Figure 8, that might bind to a common subsite. However, the molecules differ dramatically at either end of the core. One end contains either a purine or pyrimidine on the ribose, and the other end contains either an *N*-acetylenolpyruvylglucosamine or a ribose nicotinamide. A single binding site would have to manage a high degree of specificity between two very different reactive substrate sites for catalysis to occur. Moreover, analogs of NADPH without the 2′- or 3′-phosphate do not bind as substrates or inhibitors. This suggests that a single binding site would require a 2′-phosphate on both substrates, or that a single

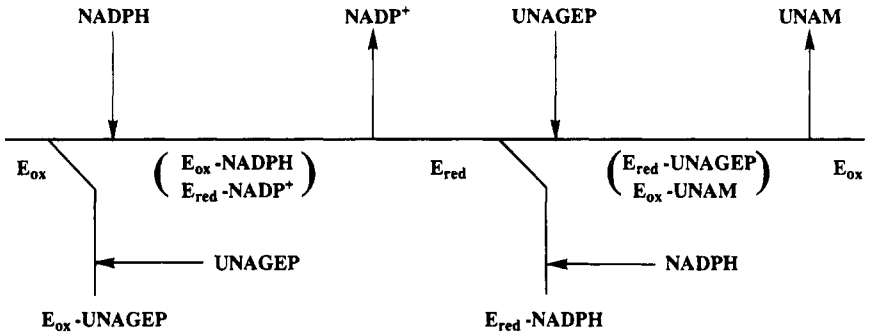

FIGURE 9: Proposed steady-state kinetic mechanism of UDP-*N*-acetylenolpyruvylglucosamine reductase.

site would have to exist in two forms in order to accommodate both NADPH and UDP-*N*-acetylenolpyruvylglucosamine. Alternatively, the enzyme might contain two sites that share a common subsite, which would be consistent with the data in Figure 6.

Substrate inhibition is common in ping pong mechanisms, and double competitive substrate inhibition has been observed in other enzymes including nucleoside diphosphate kinase (Garces & Cleland, 1969), *O*-acetylserine sulfhydrylase (Cook & Wedding, 1976), and thiolase (Stewart & Rudney, 1966). Substrate inhibition generally is the result of substrates combining with improper forms of the enzyme that result in dead-end complexes. Alternatively, the same rate profiles can be observed if the kinetic mechanism involves random addition of A and B, and there is a kinetically preferred pathway that can be overcome at high concentrations of one substrate (Ferdinand, 1966). The relatively strong substrate inhibition by UNAGEP in comparison to NADPH might suggest such a preferred kinetic pathway. However, the pattern of parallel lines that converge and change slope in Figure 4 is not consistent with a sequential mechanism requiring both substrates to form a ternary complex, and therefore, a preferred pathway can be ruled out. The data are consistent with a ping pong mechanism and indicate that substrate inhibition is the result of substrates combining with improper enzyme forms.

Substrate inhibition by both substrates provided the additional constraint that the overall kinetic mechanism would have to account for double substrate inhibition. This, in fact, was observed when the initial velocity patterns as a function of both substrates were obtained, as shown in Figure 4. The initial velocity patterns were consistent with a ping pong bi bi double competitive substrate inhibition mechanism. The same mechanism was observed at pH 7.0, 8.0, and 9.0, although the relative degree of substrate inhibition for each substrate varied as a function of pH. The k_{cat}s obtained from these data provide lower limits for the slowest microscopic rate constant in the mechanism. Based on the k_{cat}s, the slowest step cannot be any slower than between 40 and 60 s^{-1} at 37 °C, depending on the pH.

Figure 9 illustrates the individual steps in the proposed mechanism for UDP-*N*-acetylenolpyruvylglucosamine reductase. The mechanism proposes release of $NADP^+$ before addition of UNAGEP, and the exchange reaction illustrated in Figure 7 provided support for this. The mechanism also proposes that each of the substrates forms a dead-end complex with the form of the enzyme involved in binding the other substrate.

In general, dead-end complexes may result from two substrates competing for a single enzyme binding site that exists in two forms, or one substrate binding at two sites in a two site enzyme. In the classical case, both substrates compete for a single enzyme site. In the nonclassical case, one or both substrates can bind to the site for the other substrate. The classical case can be envisioned easily in terms of a stable enzyme intermediate, where the first substrate donates a functional group to the enzyme and the second substrate binds at the same site and accepts the group, such as in nucleoside diphosphate kinase (Garces & Cleland, 1969). Substrate inhibition would result from the second substrate binding prior to formation of the intermediate. The nonclassical case can be understood in terms of mobile intermediates where the enzyme shuttles a functional group between two sites, such as in enzymes containing biotin (Northrop & Wood, 1969; Barden et al., 1972) or lipoic acid (Tsai et al., 1973). Here, substrate inhibition would result from one substrate binding to both sites.

A flavoprotein intermediate might function in either a one site or a two site enzyme. Two site nonclassical enzymes are known wherein the transfer between sites occurs through a reduced flavoprotein intermediate, such as in glutamate synthetase (Rendina & Orme-Johnson, 1978) or glutathione reductase (Bulger & Brandt, 1971a,b). For glutamate synthetase, the measured product inhibition patterns (Rendina & Orme-Johnson, 1978) are different from the predicted patterns for a ping pong bi bi uni uni mechanism with one catalytic site (Barden et al., 1972), and the measured patterns have been used to conclude that there are two separate substrate sites on glutamate synthetase. In the case of glutathione reductase, the measured individual rate constants are inconsistent with both substrates having to bind at the same site (Bulger & Brandt, 1971), and in fact, solution of the crystal structure has demonstrated the presence of two binding sites (Pai & Schulz, 1983). The product and analog inhibition patterns for UDP-*N*-acetylenolpyruvylglucosamine reductase suggested a double inhibition experiment that provided evidence of mutually exclusive substrate binding (see below).

The proposed mechanism for UDP-*N*-acetylenolpyruvylglucosamine reductase in Figure 9 predicts that $NADP^+$ will be a competitive inhibitor against UNAGEP because they both bind to the same form of the enzyme. The observed pattern was noncompetitive with substrate inhibition. The noncompetitive pattern is evidence that $NADP^+$ can partially reverse the reaction by reoxidizing the flavin. Products that can reverse an enzyme reaction decrease the proportion of central complexes that go on to products, and hence they display noncompetitive inhibition because the varied substrate cannot overcome the conversion to a separate enzyme form (Cleland, 1986).

Inhibition by $NADP^+$ was noncompetitive with respect to NADPH, as would be expected because it does not bind to the E_{ox} form of the enzyme as does NADPH. The $APADP^+$ analog gave competitive inhibition versus NADPH. Competitive inhibition by $APADP^+$ indicates that $APADP^+$ and NADPH can bind to the same form of the enzyme, which is most likely the oxidized form because NADPH demonstrated only weak substrate inhibition and therefore does not combine well with reduced enzyme. By comparison, $NADP^+$ and $APADP^+$ are sterically very similar, but differ in the extent of delocalized charge in the pyridine ring. The nicotinamide end of the molecule must interact with the flavin during catalysis, and thus the electrostatic change may define a binding determinant at or very near the flavin that allows it to bind to the oxidized form.

Similarly, UNAG was a competitive inhibitor against UNAGEP, where the difference is that UNAG does not contain the enolpyruvyl group of UNAGEP. However, the K_{is} was 5.7 mM as compared to the K_m of 24 μM for UNAGEP. Whether the difference in the constants is due to binding energy or stabilization of a transition state structure, the enolpyruvyl group must provide an important interaction at or near the flavin. In this regard, UNAM was a poor product inhibitor, with a K_{ii} of 8.4 mM. Reduction of UNAGEP to UNAM creates two sp^3 hybridized carbons in the product, and thus eliminates the planarity of the substrate at the enolpyruvyl moiety. The poor binding of UNAG, without the enolpyruvyl moiety, and the poor binding of UNAM, wherein the enolpyruvyl has been reduced and converted to sp^3 geometry, together demonstrate that the enzyme achieves a high degree of specificity in the planar configuration around the enolpyruvyl functional group.

In combination, the inhibition experiments identified $APADP^+$ and UNAG as two molecules that define binding interactions at or near the flavin. This suggested the possibility of performing a double inhibition experiment with $APADP^+$ and UNAG to determine whether or not these molecules exhibit mutually exclusive interactions on the enzyme. The results in Figure 6 show that they do. Assuming that $APADP^+$ and UNAG are representative of NADPH and UNAGEP by virtue of being competitive inhibitors, the double inhibition experiment suggests that NADPH and UNAGEP share the same binding site, or at least a subsite that makes their binding mutually exclusive (Segel, 1975). Furthermore, the reciprocal dependence of substrate inhibition on pH, as mentioned above, might be related to a functional group regulating binding at a common subsite.

The sequence of the MurB gene has been analyzed for the presence of folding motifs that might suggest a common subsite. The common dinucleotide portions of NADPH and UNAGEP, and the presence of tightly bound FAD, immediately pointed to the possibility of one or more Rossmann folds in the protein (Rossmann et al., 1975). However, the sequence does not contain the classical Gly-X-Gly-X-X-Gly or any of its variants that might suggest a dinucleotide fold (Schulz, 1992). The sequence also demonstrates very low homology to other proteins in the Swiss Protein Databank. Consequently, there are no obvious structural hints on the nature of a possible substrate site or subsite in the protein. The goal of future experiments will be to expand our knowledge of the binding properties of the enzyme and to obtain a complete description of the individual rate constants in the kinetic mechanism.

ACKNOWLEDGMENT

We thank Ann Starrett and Bethanne Warrack for mass spectroscopic analysis of the substrates and products, and Dr. Mark Hail for mass spectroscopic analysis of purified enzyme.

REFERENCES

Anwar, R. A., & Vlaovic, M. (1979) Purification of UDP-N-Acetylenolpyruvylglucosamine Reductase from *Escherichia coli* by Affinity Chromatography, Its Subunit Structure and the Absence of Flavin as the Prosthetic Group. *Can. J. Biochem. 57*, 188−196.

Barden, R. E., Fung, C.-H., Utter, M. F., Scrutton, M. C. (1972) Pyruvate Carboxylase from Chicken Liver Steady-State Kinetic Studies Indicate a "Two-Site" Ping-Pong Mechanism. *J. Biol. Chem. 247*, 1323−1333.

Benson, T. E., Marquardt, J. L., Marquardt, A. C., Etzkorn, F. A., & Walsh, C. T. (1993) Overexpression, Purification, and Mechanistic Study of UDP-N-Acetylenolpyruvylglucosamine Reductase. *Biochemistry 32*, 2024−2030.

Benson, T. E., Walsh, C. T., & Hogle, J. M. (1994) Crystallization and Preliminary X-ray Crystallographic Studies of UDP-N-Acetylenolpyruvylglucosamine Reductase. *Protein Sci. 3*, 1125−1127.

Bugg, T. D. H., & Walsh, C. T. (1992) Intracellular Steps of Bacterial Cell Wall Peptidoglycan Biosynthesis: Enzymology, Antibiotics, and Antibiotic Resistance. *Nat. Prod. Rep. 9*, 199−215.

Bulger, J. E., & Brandt, K. G. (1971a) Yeast Glutathione Reductase I Spectrophotometric and Kinetic Studies of its Interaction With Reduced Nicotinamide Adenine Dinucleotide. *J. Biol. Chem. 246*, 5570−5577.

Bulger, J. E., & Brandt, K. G. (1971b) Yeast Glutathione Reductase II Interaction of Oxidized and 2-Electron Reduced Enzyme with Reduced and Oxidized Nicotinamide Adenine Dinucleotide Phosphate. *J. Biol. Chem. 246*, 5578−5587.

Cleland, W. W. (1986) in *Investigations of Rates and Mechanisms of Reaction* (Bernasconi, C., Ed.) Vol. 6, pp 791−870, Wiley, New York.

Cleland, W. W. (1990) in *The Enzymes, Third Edition* (Sigmon, D. S., & Boyer, P. D., Eds.) Vol. 19, pp 99−158, Academic Press, San Diego.

Cook, P. F., & Wedding, R. T. (1976) A Reaction Mechanism from Steady State Kinetic Studies for O-Acetylserine Sulfhydrylase from *Salmonella typhimurium* LT-2. *J. Biol. Chem. 251*, 2023−2029.

Falk, P. J. (1994) Purification, Characterization, and Comparison of UDP-N-Acetylenolpyruvoylglucosamine Reductase from *E. coli.* JM109 pBS::*murB* and *E. coli.* JM109 pMa1C2::*murB* Fusion Protein, Master's Thesis, Quinnipiac College.

Ferdinand, W. (1966) The Interpretation of Non-Hyperbolic Rate Curves for Two-Substrate Enzymes. *Biochem. J. 98*, 278.

Garces, E., & Cleland, W. W. (1969) Kinetic Studies of Yeast Nucleoside Diphosphate Kinase. *Biochemistry 8*, 633−640.

Ikeda, M., Wachi, M., Jung, H. K., Ishino, F., & Matsuhashi, M. (1990a) Nucleotide Sequence Involving murG and murC in the mra Gene Cluster Region of *Escherichia coli. Nucleic Acids Res. 18*, 4014.

Ikeda, M., Wachi, M., Ishino, F., & Matsuhashi, M. (1990b) Nucleotide Sequence Involving murD and an Open Reading Frame ORF-y Spacing murF and ftsW in *Escherichia coli. Nucleic Acids Res. 18*, 1058.

Marquardt, J. L., Siegele, D. A., Kolter, R., & Walsh, C. T. (1992) Cloning and Sequencing of *Escherichia coli* murZ and Purification of its Product, a UDP-N-Acetylglucosamine Enolpyruvyl Transferase. *J. Bacteriol. 174*, 5748−5752.

Mengin-Lecreulx, D., & van Heijenoort, J. (1990) Nucleotide Sequence of the murD Gene Encoding the UDP-MurNAc-L-Ala-D-Glu Synthetase of *Escherichia coli. Nucleic Acids Res. 18*, 183.

Northrop, D. B., & Wood, H. G. (1969) Transcarboxylase VII Exchange Reactions and Kinetics of Oxalate Inhibition. *J. Biol. Chem. 244*, 5820−5827.

Pai, E. F., & Schulz, G. E. (1983) The Catalytic Mechanism of Glutathione Reductase as Derived from X-Ray Diffraction Analyses of Reaction Intermediates. *J. Biol. Chem. 258*, 1752−1757.

Pucci, M. J., Discotto, L. F., & Dougherty, T. J. (1992) Cloning and Identification of the *Escherichia coli* murB DNA Sequence, Which Encodes UDP-N-Acetylenolpyruvoylglucosamine Reductase. *J. Bacteriol. 174*, 1690−1693.

Rendina, A. R., & Orme-Johnson, W. H. (1978) Glutamate Synthase: On the Kinetic Mechanism of the Enzyme from *Escherichia coli* W. *Biochemistry 17*, 5388−5393.

Rossmann, M. G., Liljas, A., Branden, C. I., & Banaszak, L. J. (1975) Evolutionary and Structural Relationships Among Dehydrogenases. In *The Enzymes* (Boyer, P. D., Ed.) Vol. 11, pp 61−102, Academic Press, New York.

Schulz, G. E. (1992) Binding of Nucleotides by Proteins. *Curr. Opin. Struct. Biol. 2*, 61−67.

Segel, I. H. (1975) Enzyme Kinetics Behavior and Analysis of Rapid Equilibrium and Steady-State Enzyme Systems, pp 780, 829, John Wiley & Sons, New York.

Stewart, P. R., & Rudney, H. (1966) The Biosynthesis of β-Hydroxy-β-Methylglutaryl Coenzyme A in Yeast III Purification and Properties of the Condensing Enzyme Thiolase System. *J. Biol. Chem. 241*, 1212−1221.

Suelter, C. H. (1970) Enzymes Activated by Monovalent Cations. *Science 168*, 789−795.

Taku, A., Gunetileke, K. G., & Anwar, R. A. (1970) Biosynthesis of Uridine Diphospho-N-acetylmuramic Acid III Purification and Properties of Uridine Diphospho-N-Acetylenolpyruvylglucosamine Reductase. *J. Biol. Chem. 245*, 5012−5016.

Tsai, C. S., Burgett, M. W., & Reed, L. J. (1973) α-Keto Acid Dehydrogenase Complexes XX. A Kinetic Study of the Pyruvate Dehydrogenase Complex from Bovine Kidney. *J. Biol. Chem. 248*, 8348−8352.

BI942779T